

Constraining aerosol single scattering albedos from multiangle, multispectral photo-polarimetric observations over the ocean

J. Chowdhary^a, B. Cairns^a, M. I Mishchenko^b, and L. D Travis^b

^aDept. of Appl. Phys. and Appl. Math., Columbia University, 2880 Broadway, New York, NY USA

^bNASA/Goddard Institute for Space Studies, 2880 Broadway, New York, NY USA

ABSTRACT

The extensive set of measurements performed during the Chesapeake Lighthouse and Aircraft Measurements for Satellites (CLAMS) experiment provides a unique opportunity to evaluate aerosol retrievals over the ocean from multiangle, multispectral photometric and polarimetric remote sensing observations by the airborne Research Scanning Polarimeter (RSP) instrument. Previous studies have shown the feasibility of retrieving particle size distributions and real refractive indices from such observations for visible wavelengths without prior knowledge of the ocean color. This work evaluates the fidelity of the aerosol retrievals using RSP measurements during the CLAMS experiment against aerosol properties derived from *in-situ* measurements, sky radiance observations and sunphotometer measurements, and further extends the scope of the RSP retrievals by using *a priori* information about the ocean color to constrain the aerosol absorption. Satisfying agreement is found for all aerosol products.

Keywords: Remote sensing, polarization, aerosol retrieval, ocean modeling, radiative transfer

1. INTRODUCTION

Aerosols can change the radiative budget of the atmosphere by scattering or absorbing sunlight (“direct climate forcing”) and by modifying the formation and life-cycle of clouds (“indirect climate forcing”). To evaluate the magnitude of these climate forcings requires accurate retrievals of the particle size, complex refractive index, and number density of aerosols¹. In a recent article² we explored the estimation of aerosol properties from visible polarized reflectances obtained over the ocean by the Research Scanning Polarimeter (RSP) instrument³, an airborne remote sensor that is functionally similar to the Earth Observing Scanning Polarimeter (EOSP) instrument⁴. We demonstrated that the polarized reflectance near the backscattering direction is essentially insensitive to light emerging from the ocean body which enabled us to separate the ocean color from aerosol scattering contributions in the remote sensing of visible (VIS) radiances. We then applied this observation to constrain the effective radius r_e and effective variance v_e of the fine-mode aerosol component as well as the real refractive index $\text{Re}[m_f]$ of this aerosol. In this paper, we extend our analysis to include an evaluation of how well the aerosol single scattering albedo ω_f of fine-mode aerosols can be estimated from RSP measurements over the ocean.

The rationale for our approach is based on using the aerosol estimates from polarized reflectance measurements in the VIS to fit the corresponding total reflectance measurements. Hence the assumption made here is that latter reflectance is much more sensitive to ω_f than the former reflectance, the validity of which can be checked beforehand from the estimates of r_e , v_e and of $\text{Re}[m_f]$. Over the ocean, one has to account further for the contribution of waterleaving radiances to the total reflectance. To correct for this contribution, we propose using the total reflectance spectral and angular measuring capabilities of the RSP instrument to simultaneously constrain ω_f and the ocean color. Away from coastal regions, one can parameterize this color in terms of the concentration [Chl] of chlorophyll *a* which is a photosynthetic pigment found in phytoplankton⁵. The retrieval over open oceans of ω_f from total reflectance measurements will therefore depend on the value assumed for [Chl], and the correct value of [Chl] should yield a smooth variation of the aerosol absorption coefficient, k_{abs} , in the VIS. The situation is more complicated for coastal regions, where the discharge and resuspension of sediments and colored dissolved organic matter from freshwater runoff can cause significant changes in the ocean color⁶. Here, one may use instead reflectance measurements of the upwelling radiance just above the ocean surface and/or measurements of the underwater light scattering properties to constrain the ocean color.

We use for the analyses in this paper data obtained from the Chesapeake Lighthouse and Aircraft Measurements for Satellites (CLAMS) experiment, which took place during the period of July 10 to August 2, 2001. The CLAMS experiment was a short-wave radiative closure experiment that involved measurements obtained from six research aircraft, several land sites, and an ocean platform. Its goal was to validate and improve atmospheric and oceanic products retrieved from observations onboard the spacecraft Terra by the Clouds and Earth's Radiant Energy System (CERES) instrument, the Multi-angle Imaging Spectro-Radiometer (MISR) instrument, and the MODerate Resolution Imaging Spectroradiometer (MODIS) instrument. The majority of the measurements were centered close to the Chesapeake Lighthouse research platform, which is located 25 km east of Virginia Beach and which functions as the CERES Ocean Validation Experiment (COVE) site where radiation, meteorology, and ocean optics are monitored continuously. One component of the CLAMS' field campaign consisted of operating the RSP instrument onboard a Cessna 210 aircraft to measure Stokes parameters I , Q , and U of the upwelling radiation as a function of wavelength and viewing angle. Other components of the CLAMS experiment that are of interest to the present analyses are the aerosol and skylight measurements by instruments onboard the University of Washington Convair-580 research aircraft⁷, the ocean optics measurements performed from the COVE ocean platform⁸, and the skylight measurements made by the AERosol Robotic NETwork (AERONET)⁹. The CLAMS experiment is therefore ideally suited to study the retrieval of aerosol scattering and absorption properties from RSP observations over oceans.

2. POLARIZATION OF THE EARTH'S REFLECTANCE OVER OCEANS

2.1 Sensitivity to aerosols

The linear polarization of light observed over the ocean from an aircraft or spacecraft contains a wealth of information that is not readily available from total radiance data. Light, in its most general form, can be described as the sum of an unpolarized component and a fully polarized component. Linearly polarized light makes up most of the latter component (with typically only a very tiny fraction of circular polarized light), and originates in atmosphere-ocean systems predominantly from particle scattering in the atmosphere and ocean and from skylight reflection by the ocean surface. Both the total and polarized radiance exhibit features as a function of scattering angle and wavelength that can be used to extract information about the atmosphere and the ocean. However, the polarized radiance features are generally much sharper, more numerous, and show larger variations than total radiance features because of their large sensitivity to particle properties and weak sensitivity to multiple scattering. Another advantage of including polarization in the remote sensing of the atmosphere and the ocean is that the degree of polarization (ratio of polarized radiance to total radiance) is independent of instrumental calibration, i.e., the uncertainty in this polarization ratio is much smaller than the one for radiance measurements.

*Hansen and Travis*¹⁰ give numerous results for the polarization of light scattered by planetary atmospheres. Figure 1 provides additional results relevant to the topic of this paper. Let $F(\Theta)$ be the matrix that describes scattering of light by a small volume element of the atmosphere containing randomly oriented particles. The first row in Fig. 1 shows then the scattering function $F_{11}(\Theta)$ (panel *a*) and the degree of linear polarization $-F_{21}(\Theta)/F_{11}(\Theta)$ (panel *b*) for various non-absorbing, spherical fine-mode particles. The effective radius r_e of the particle size distribution is either 0.15 or 0.30 μm , and we vary the refractive index $\text{Re}[m_f]$ from 1.35 to 1.55 for each r_e . The effective variance v_e of the particle size distribution remains fixed at 0.1, and the wavelength λ of light is 550 nm. Note further that $\varpi_f = 1$. Of interest are the following observations. First, both the scattering function and degree of linear polarization are sensitive to variations in r_e for given $\text{Re}[m_f]$, but the change in degree of linear polarization involves new angular features and even reversal of signs. Secondly, changing $\text{Re}[m_f]$ affects both the scattering function and degree of linear polarization for $r_e = 0.3 \mu\text{m}$, but this sensitivity becomes small for the scattering function if r_e approaches 0.15 μm . Finally, the scattering function is much more sensitive to r_e than to $\text{Re}[m_f]$ for scattering angles close to 0° . The polarization of light scattered in the backward and forward direction by a small volume element of the atmosphere is on the other hand zero for all r_e and $\text{Re}[m_f]$, i.e., polarization observed for these angles must be scattered more than once.

Panels *c* and *d* of Fig. 1 show the same results as panels *a* and *b* except for keeping $\text{Re}[m_f]$ fixed at 1.45 and changing ϖ_f . Deviations of ϖ_f from unity in the visible part of the spectrum are usually considered to be caused by the presence in aerosol mixtures of strongly absorbing soot impurities. Such impurities can exist either outside or inside non-absorbing particles, the latter of which is the case for soot particles scavenged by liquid droplets. In what follows, we adopt non-zero values for the imaginary part of the fine-mode particle refractive index $\text{Im}[m_f]$ to simulate changes in ϖ_f . Hence, the assumption here is that the absorbing and non-absorbing aerosol components are internally mixed. The values chosen for $\text{Im}[m_f]$ are 0.00, 0.01, and 0.02, which leads to $\varpi_f = 1.0$, 0.94, and 0.88 for $r_e = 0.15 \mu\text{m}$ and to

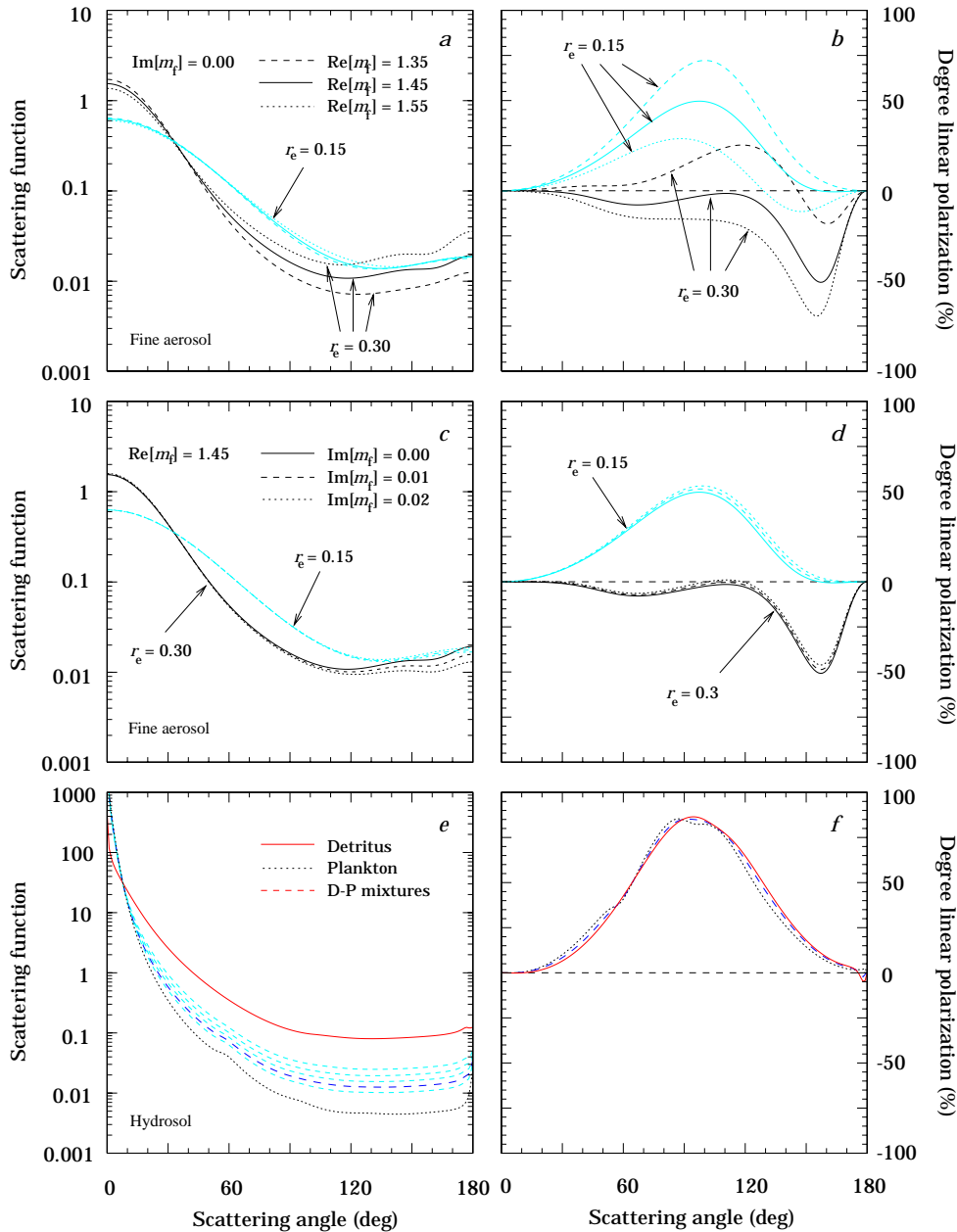


Fig. 1. Scattering functions (left column) and degrees of linear polarization (right column) for various fine-mode aerosol particles (first and second rows) and for mixtures of detritus and plankton particles (third row). The light dashed lines in the third row are for $[\text{Chl}] = 0.03, 0.1, 0.3, 1.0, \text{ and } 3.0 \text{ mg/m}^{-3}$. The dark dashed line in this row corresponds to the mixture used for the analyses of RSP data in Sec. 5, and coincides with $[\text{Chl}] = 0.1 \text{ mg/m}^{-3}$.

1.0, 0.95, and 0.90 for $r_e = 0.3 \text{ }\mu\text{m}$, respectively. The results in the second row of Fig. 1 show that the sensitivity of scattering function and degree of linear polarization to $0.00 \leq \text{Im}[m_f] \leq 0.02$ is small to negligible. Most of the variation of the Earth's reflectance with $\bar{\omega}_f$ must therefore originate from multiple scattering events. Hansen and Travis¹⁰ demonstrate further that the polarized reflectance of a planetary atmosphere is much less susceptible to multiply scattered light than the corresponding total reflectance. This observation, combined with the results shown in Fig. 1, constitutes the basis for our rationale of using the Earth's polarized reflectance to retrieve r_e , v_e , and $\text{Re}[m_f]$ and of subsequently using the Earth's total reflectance to constrain $\bar{\omega}_f$.

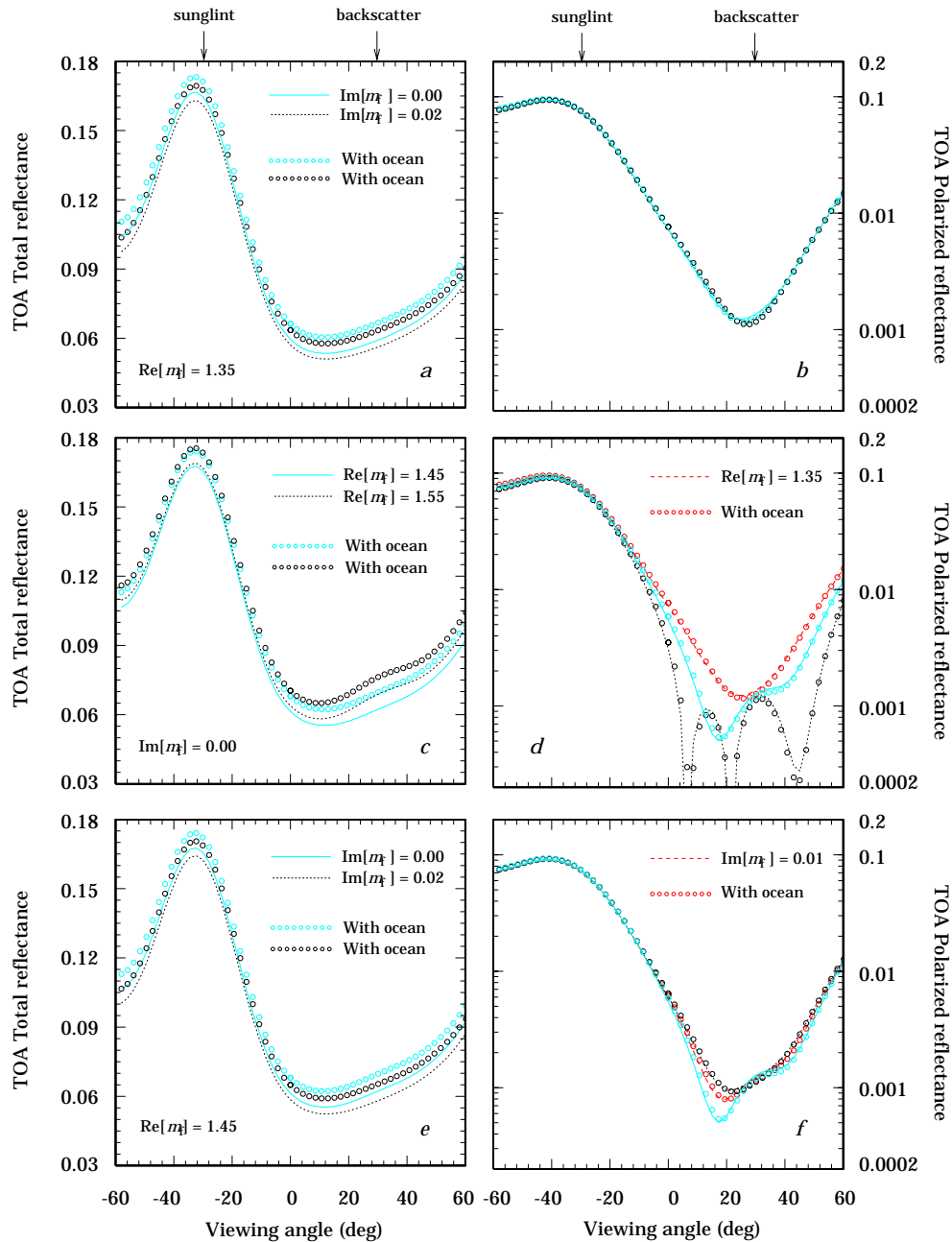


Fig. 2. Model results for the total reflectance (left column) and polarized reflectance (right column) of light emerging from the top of the atmosphere for various atmosphere-ocean system case studies. Lines and open circles are for ignoring and including the contribution of light emerging from an open ocean with $[\text{Chl}] = 1.0 \text{ mg/m}^{-3}$, respectively.

2.2 Model simulations

The simulations performed for the present work use the scattering models and numerical techniques described by Chowdhary *et al.*¹¹ for radiative transfer computations of polarized light in atmosphere-ocean systems. Here, we provide only a brief outline of these models and techniques.

The models used for the scattering properties of the atmosphere and ocean surface are similar to the ones in Chowdhary *et al.*². That is, we mix the aerosols particles homogeneously with molecules up to a height of 3.6 km, above which the atmosphere consists of molecules only. For simplicity, we consider fine-mode aerosols only, i.e., there are no coarse-mode aerosol particles present. Gaseous absorption is assumed to occur above the aerosol layer by

an ozone amount of 332 Dobson units. For the ocean surface we use the wind-ruffled slope-distribution of *Cox and Munk*¹², correct for shadowing effects following *Sancer*¹³, and account for scattering by ocean foam as in *Koepke*¹⁴ and *Frouin et al.*¹⁵. Note that we include the effects of wind-direction on the reflection by ocean surface of the *direct* sunlight (i.e., sunlight that is attenuated but not scattered in the atmosphere). To preserve energy lost by multiple scattering between ocean waves¹⁶ and by the discretization of underwater light directions, we use a modified version of *Hansen's*¹⁷ iterative normalization method to update the ocean surface reflection matrix and normalize the ocean surface transmission matrix along the two directions closest to the refraction peak for a smooth surface.

To account for variations in the backscattering efficiency q_p of oceanic particulates with [Chl], we use a mixture of two particulate components: phytoplankton and detritus particles. The approach is similar to the one used by *Morel et al.*¹⁸ except for using (i) the bimodal distribution of (real) refractive index commonly found for oceanic particulates¹⁹ for the two particulate components, and (ii) an upper limit for underwater-light polarization signatures²⁰ to constrain the size distributions and refractive indices of these components. The scattering functions and degrees of linear polarization of two such components, and of some of their so-called D-P mixtures, are shown in the third row of Fig. 1. The underwater-light polarization constraint used for these components is the linear polarization of light scattered by pure sea water²¹, i.e., of Rayleigh scattering with a depolarization factor of 0.09. Mixing such particulate components allows one not only to reproduce observed variations of particulate backscattering efficiency (panel *e*), but also to maintain the same degree of polarization regardless of the mixture (panel *f*). Adding water to this mixture further changes the scattering function but not the polarization for underwater light single scattering (cf. Fig. 3 in *Chowdhary et al.*²).

Figure 2 provides few case studies of the total reflectance (first column panels) and polarized reflectance (second column panels) computed for top-of-atmosphere (TOA) observations over the ocean at $\lambda = 550$ nm. The aerosol model for these case studies is the same as the one used for Fig. 1 with $\text{Re}[m_f] = 1.35$ and $r_e = 0.3 \mu\text{m}$, and the optical thickness τ_f of this fine-mode aerosol is 0.15. The ocean surface roughness is computed for an ocean surface wind-speed and -azimuth of 7 m/s and 90° , respectively, and waterleaving radiances are obtained for an open ocean with $[\text{Chl}] = 1.0 \text{ mg/m}^3$. The results are shown for solar principal plane observations and a solar zenith angle of 30° , and the sign of the viewing angle is positive (negative) for the backscattering (sunglint) viewing directions. Panels *a* and *b* show the variation of TOA reflectances with $\text{Im}[m_f]$ and with an ocean while keeping $\text{Re}[m_f]$ fixed at 1.35. Note that the total reflectances vary considerably with $\text{Im}[m_f]$, i.e., the change can be comparable to the intensity of waterleaving radiances especially if $[\text{Chl}] \leq 1.0 \text{ mg/m}^3$. On the other hand, the polarized reflectances show little sensitivity to both $\text{Im}[m_f]$ and the presence of an ocean. The non-zero value for the latter reflectance in the backscattering direction originates predominantly from skylight reflected off the ocean surface. For comparison, we show in panels *c* and *d* the change in TOA reflectances if $\text{Re}[m_f]$ is varied instead of $\text{Im}[m_f]$. Here, we observe large sensitivities not only for the total but also for the polarized reflectances to variations in $\text{Re}[m_f]$. However, the latter reflectances continue to vary much less with waterleaving radiances even in the vicinity of neutral points. Similar results can be obtained for $r_e = 0.15 \mu\text{m}$ although the sensitivity to $\text{Re}[m_f]$ becomes then significantly smaller. Our rationale for using angular features in the polarized reflectances to retrieve $\text{Re}[m_f]$ and r_e without prior knowledge of $\text{Im}[m_f]$ and of [Chl] works therefore fine at $\lambda = 550$ nm for $\text{Re}[m_f] \approx 1.35$ and $r_e \approx 0.30 \mu\text{m}$, and the same holds for smaller values of r_e except for reducing the accuracy of $\text{Re}[m_f]$ retrievals. Sensitivity analyses (not shown here) show that the latter retrievals can be improved by using the reflectance of polarized light at smaller wavelengths. Larger values of $\text{Re}[m_f]$ lead, on the other hand, to an increase in sensitivity of polarized reflectances to $\text{Im}[m_f]$. Such cases can be predetermined as in panels *e* and *f* of Fig. 2, and require reassessing the retrievals of $\text{Re}[m_f]$ and/or particle size distribution if $\text{Im}[m_f]$ is changed.

3. METHODOLOGY

*Chowdhary et al.*² discuss the steps involved in inverting RSP data to retrieve aerosol scattering properties. Their procedure takes advantage of the large difference in aerosol scattering optical thickness spectra for submicrometer- and micrometer-sized particles over the range of RSP-wavelengths to separate the retrieval of these particles. It starts by inverting the 2250-nm total and polarized reflectances to estimate the scattering properties of coarse mode aerosols, and uses this estimate together with the (total and) polarized reflectance measurements at $\lambda \leq 865$ nm to constrain the scattering properties of fine-mode aerosols. The current case study focuses however on the estimating the scattering properties of fine-mode particles only (i.e., ignores the presence of coarse-mode aerosols), and adds the retrieval of $\overline{\omega}_f$ to its products. To accommodate for these changes, we modify the retrieval method given by *Chowdhary et al.*² as

follows. Let $\{R\}_\lambda$ and $\{P\}_\lambda$ stand for the bidirectional total and polarized RSP reflectances measured in the solar principal plane at wavelength λ , respectively. The retrieval procedure loops then through the following steps:

1. Use the *sun glint* angular profile in $\{R\}_{2250}$ to constrain the ocean surface wind-speed and -direction under the assumption of a molecular (i.e., aerosol-free) atmosphere
2. Use the *off-sun glint* data in $\{P\}_{470}$ to $\{P\}_{670}$ to obtain estimates of r_e , v_e , and $\text{Re}[m_f]$ for *non-absorbing* fine-mode particles assuming a black ocean body
3. Use the *off-sun glint* data in $\{R\}_{670}$ to obtain an estimate of τ_f for *non-absorbing* fine-mode particles assuming a black ocean body
4. Use the *off-sun glint* data in $\{R\}_{470}$ and $\{R\}_{555}$ to retrieve the ocean color using the fine-mode estimate from the previous step for atmospheric correction
5. Compare the retrieved ocean color with ocean spectra estimated from bio-optical ocean models for $0.03 \leq [\text{Chl}] \leq 3.0 \text{ mg m}^{-3}$ or from ocean optics data. If they don't match, proceed to step 6
6. Choose $\text{Im}[m_f] \neq 0$ for the aerosol estimate in step 2, and use the *off-glnt* data in $\{R\}_{670}$ to adjust τ_f assuming a black ocean
7. Use the *off-glnt* data in $\{P\}_{470}$ to $\{P\}_{670}$ to verify or renew the retrievals of r_e , v_e , and $\text{Re}[m_f]$ for $\text{Im}[m_f] \neq 0$
8. Iterate steps 5 to 8 using different values of $\text{Im}[m_f] \neq 0$ until an acceptable fit between the retrieved and pre-estimated ocean color is achieved

Steps 1–3 are described in more detail by *Chowdhary et al.*² except for ignoring coarse-mode aerosols. Note further that we do not utilize $\{R\}_{410}$ and $\{P\}_{410}$ which are sensitive to the vertical distribution of absorbing aerosols. Steps 4–5 test the assumption made in steps 2–3 of the fine-mode aerosol being non-absorbing by using the resulting aerosol estimate to compute the contribution of atmospheric scattering to remote sensing data in the VIS. Subtracting this contribution from the total reflectance data provides then an estimate of the contribution of waterleaving reflectances, the spectrum of which can be verified by comparing with known ocean spectra. In steps 6–8, we relax the condition of the fine-mode aerosol being non-absorbing by varying $\text{Im}[m_f]$, and obtain new retrievals of τ_f after verifying/adjusting the other fine-mode aerosol estimates. Note that we ignore in these steps the spectral variation of $\text{Im}[m_f]$ which in the visible is appropriate for soot, and which facilitates the inversion process.

To obtain the ocean reflectance for this study case, we use estimates of the underwater light bulk absorption (a_{blk}) and particulate backscattering (s_p) coefficients from *in-situ* measurements at the COVE site, and perform multiple scattering computations. The particulate scattering function for these computations (see dashed line in Fig. 1e) is characterized by a backscattering efficiency q_p that is 1.5 times the value found by *Ulloa et al.*²² for an open ocean with the same [Chl] as the COVE site. We use this larger-than-usual value for s_p to account for scattering by suspended matter originating from land. Note however that the albedo of the ocean does not depend much on the choice for q_p as long as one uses the correct value for s_p (see *Morel and Prieur*²³). We assume that the same is true for the ocean reflectance. Finally, assuming a black ocean (i.e., no water-leaving radiances) for $\{R\}_{670}$ in steps 3 and 6 is appropriate for air- and space-borne observations of the open ocean, but may need to be verified for large [Chl] values and/or observations close to the ocean because Chlorophyll *a* exhibits a fluorescence band centered at $\lambda = 683 \text{ nm}$.

4. RSP MEASUREMENTS

4.1 RSP instrument

The RSP instrument allows the first three Stokes parameters I , Q , and U to be measured simultaneously in nine spectral channels at each viewing angle³. This approach ensures that the spectral and polarimetric measurements in each instantaneous field of view (IFOV) see the same scene even if the underlying surface varies rapidly, or the aircraft is maneuvering. Because of vignetting by the skin of the aircraft, only 96 out of a possible 152 viewing angles are available for each scan, which, for the 0.8° contiguous IFOVs of the RSP, provides a limb-to-limb viewing angle range of 76° . Partial vignetting of the limb pixels can, for this viewing range, still be noticed in some channels. The scanning of a scene occurs by means of a rotating polarization-insensitive two-mirror system that generally had its scan plane oriented along the direction of travel of the aircraft during the CLAMS field experiment. The speed of the aircraft is adjusted so that at high altitudes ($> 3 \text{ km}$) successive nadir views are one IFOV apart and the same point at the ground is seen from multiple viewing angles. The centers (full width at half maximum, FWHM) of the RSP

spectral bands are 410 (30), 470 (20), and 555 (20) nm for visible light where scattering by molecules and sub-micron aerosols is significant; 670 (20), 865 (20) and 960 (20) nm for near-infrared light where scattering by fine-mode and coarse-mode aerosols predominates; and 1590 (60), 1880 (90), and 2250 (120) nm for short-wave infrared light which is dominated by coarse-mode aerosol scattering. The radiance measurements have a wide dynamic range (effective number of bits is 14) and high signal-to-noise ratio (2000 at a Lambertian equivalent reflectance of 0.3) with a radiometric and polarimetric uncertainty of $\leq 3.5\%$ and $\leq 0.2\%$, respectively³. The total reflectance R and polarized reflectance P analyzed in this study are obtained by $\pi I (\mu_0 S)^{-1}$ and $\pi(Q^2+U^2)^{1/2} (\mu_0 S)^{-1}$, respectively, where μ_0 is the cosine of the solar zenith angle θ_0 and S is the modified extraterrestrial solar irradiance. The latter irradiance is the RSP instrument spectral response convolved with the solar spectral irradiance described by *Lean*²⁴ for a point in the solar cycle mid way between solar min and solar max.

4.2 RSP data

The RSP instrument participated in the CLAMS experiment from 10 July to 17 July 2001. More than 150 files of flight track data were acquired during this period over ocean near the COVE site and over land crossing the Dismal Swamp (available at http://www.giss.nasa.gov/data/rsp_air/clamsindex.html). RSP data were acquired at high (3.6 km) and low (60 m) altitudes. The low altitude measurements were designed to meet the desire of the CERES, MODIS and MISR teams for better characterization of the surface bidirectional reflectance distribution function (BRDF) and the high altitude measurements were designed to study the retrieval of aerosol properties from satellite observations. It was assumed that most of the aerosol burden resides below the high-altitude flight paths. Both the low and high altitude observations were obtained at a range of solar azimuth angles (0° , 45° , 90° , 135° , 180°), which allows for (i) the study of BRDF properties of the underlying surface, and (ii) the evaluation of polarimetric aerosol retrievals for a range viewing geometries. Some spiral ascents and descents were also recorded and these can be used to study the vertical distributions of aerosol properties. Occasionally, the RSP scan was oriented perpendicular (as opposed to along) the aircraft ground track which effectively turned the instrument into a push-broom imager.

We use for this study RSP data acquired on July 17th, 2001, near the Chesapeake Lighthouse platform. AERONET data obtained from this platform revealed large fine-mode aerosol optical depths, which allow us to ignore coarse-mode aerosols in the analyses of VIS reflectances. The RSP instrument recorded for this day a total of 46 data files, of which 20 were obtained near the COVE site. To constrain the properties of aerosols that are close in space and time to measurements of the sky- and underwater-light performed from the Chesapeake Lighthouse platform, we use the data collected during RSP flight 027. The ground track for this flight grazed the COVE site between 1616 to 1618 UTC, which encompasses the aerosol optical depth measurements by AERONET at 1617 UTC and is closest to the site of ocean optics measurements obtained at 1605 UTC. It crosses further the ground track of Convair-580 flight 1874 a few minutes ahead of time. The cruising height of RSP flight 027 was 3.6 km, and the RSP scan plane was oriented in the solar principal plane during this flight. The solar zenith angle for this flight was about 19° .

5. AEROSOL RESULTS

5.1 Retrieval

In what follows, we analyze only a subset of the 391 consecutive RSP scans obtained during RSP flight 027, namely, a set of 100 consecutive scans obtained when the aircraft was closest to the COVE site. We show for these scans only the combined standard deviation of a calibration uncertainty estimate of 3.5% and of the scan-to-scan variation of measurements. Table 1 summarizes our aerosol retrievals.

TABLE 1. Fine-mode aerosol retrieval from RSP flight 027.

λ (nm)	$\text{Im}[m_f] = 0.00$ ^{a)}			$\text{Im}[m_f] = 0.01$ ^{a)}			$\text{Im}[m_f] = 0.02$ ^{a)}		
	$\text{Re}[m_f]$	$\overline{\omega}_f$	τ_f	$\text{Re}[m_f]$	$\overline{\omega}_f$	τ_f	$\text{Re}[m_f]$	$\overline{\omega}_f$	τ_f
470	1.44	1.000	0.364	1.44	0.941	0.404	1.44	0.889	0.442
555	1.44	1.000	0.265	1.44	0.936	0.298	1.44	0.879	0.329
670	1.44	1.000	0.175	1.44	0.926	0.200	1.44	0.861	0.225

^{a)} $r_c = 0.15 (\pm 0.025) \mu\text{m}$, $v_c = 0.2 (\pm 0.025)$.

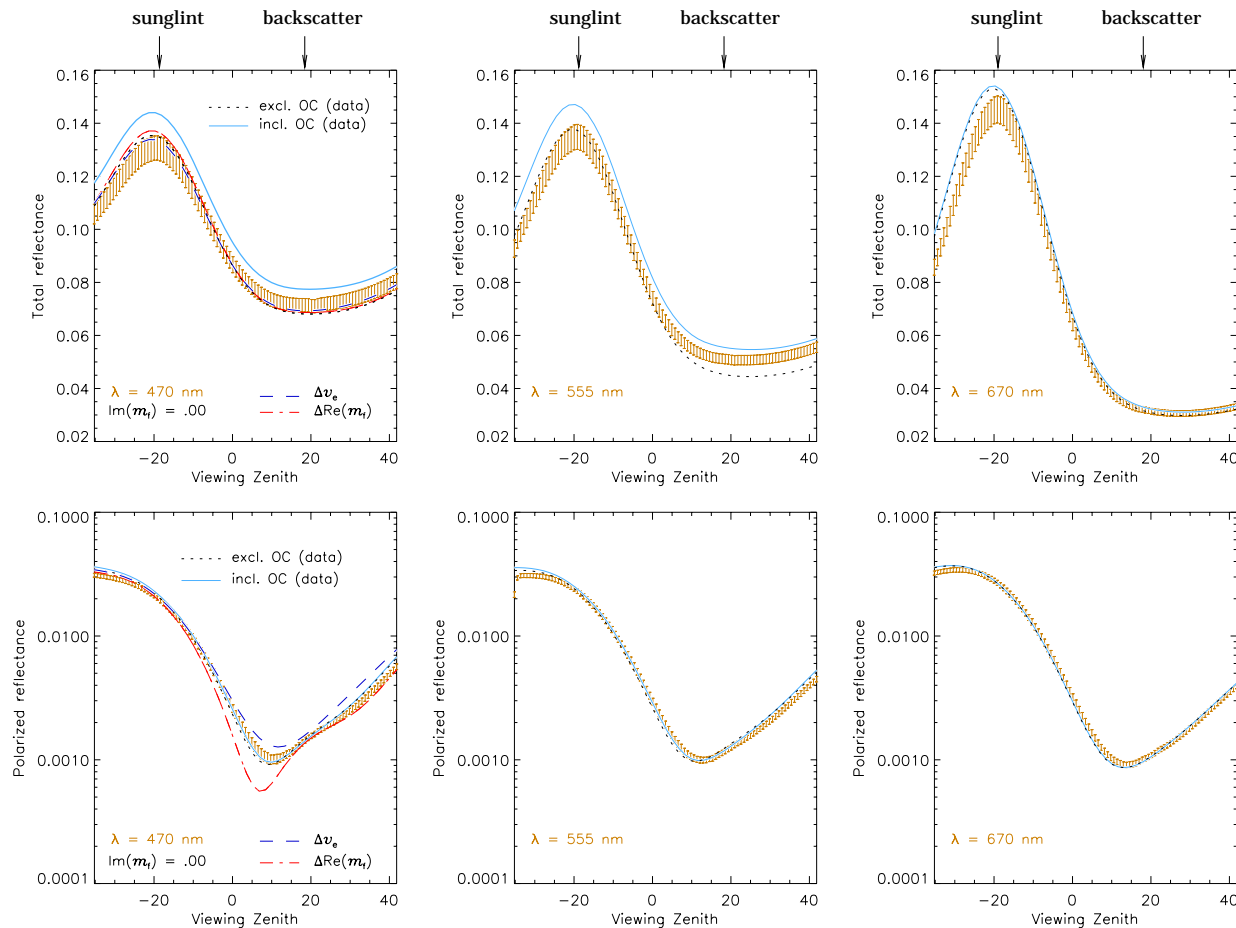


Fig. 3. Analyses of the sensitivity of RSP data to contributions from the ocean color (OC) and to variations in the scattering properties of aerosols. The error bars denote the combined standard deviation of total reflectance (first row) and polarized reflectance (second row) measured by the RSP instrument at $\lambda = 470$ nm (first column), 555 nm (second column), and 670 nm (third column). The dotted and solid curves are the numerical results for a black ocean and for and for the ocean color derived from underwater-light measurements, respectively. The properties of the aerosol model used for these results are given in Table 1 for $\text{Im}[m_f] = 0.00$. The dashed and dash-dotted curves are the numerical results for perturbations in the aerosol size distribution and real refractive index, respectively.

The panels in Fig. 3 show the results of our retrieval for non-absorbing particles. The first and second row are for the total and polarized reflectances at $\lambda = 470$ nm (first column), 555 nm (second column), and 670 nm (third column). The error bars show the combined standard deviation of RSP data. The black dotted lines show the numerical results for a black ocean (i.e., ignoring underwater light scattering) and a fine-mode aerosol characterized by $r_c = 0.15$ μm , $v_e = 0.2$, $\text{Re}[m_f] = 1.44$, and $\text{Im}[m_f] = 0.00$ (see Table 1). The solid lines show the corresponding numerical results if one includes contributions from underwater light scattering. For comparison, we include for the black-ocean case study also numerical results for perturbations in the particle size distribution ($\Delta v_e = -0.1$; see dashed line) or real refractive index ($\Delta \text{Re}[m_f] = +0.05$; see dash-dotted line). Note that we changed the optical thicknesses for the aerosol perturbation case studies to fit the total reflectance measurements at $\lambda = 670$ nm. Of interest are the following observations. First, the underwater light contribution computed for the total reflectance at $\lambda = 670$ nm is smaller than the measurement uncertainty in the corresponding RSP reflectances. This allows for the use of these reflectances to estimate the fine-mode aerosol optical thickness τ_f (step 3 in Sec. 3), although it should be noted that our underwater light computations do not account for fluorescence. That is, the fine-mode AOT may be somewhat overestimated if fluorescence by chlorophyll *a* contributes significantly to the RSP reflectances. Secondly, the underwater light contribution computed for the polarized reflectances is smaller than the measurement uncertainty in the corresponding

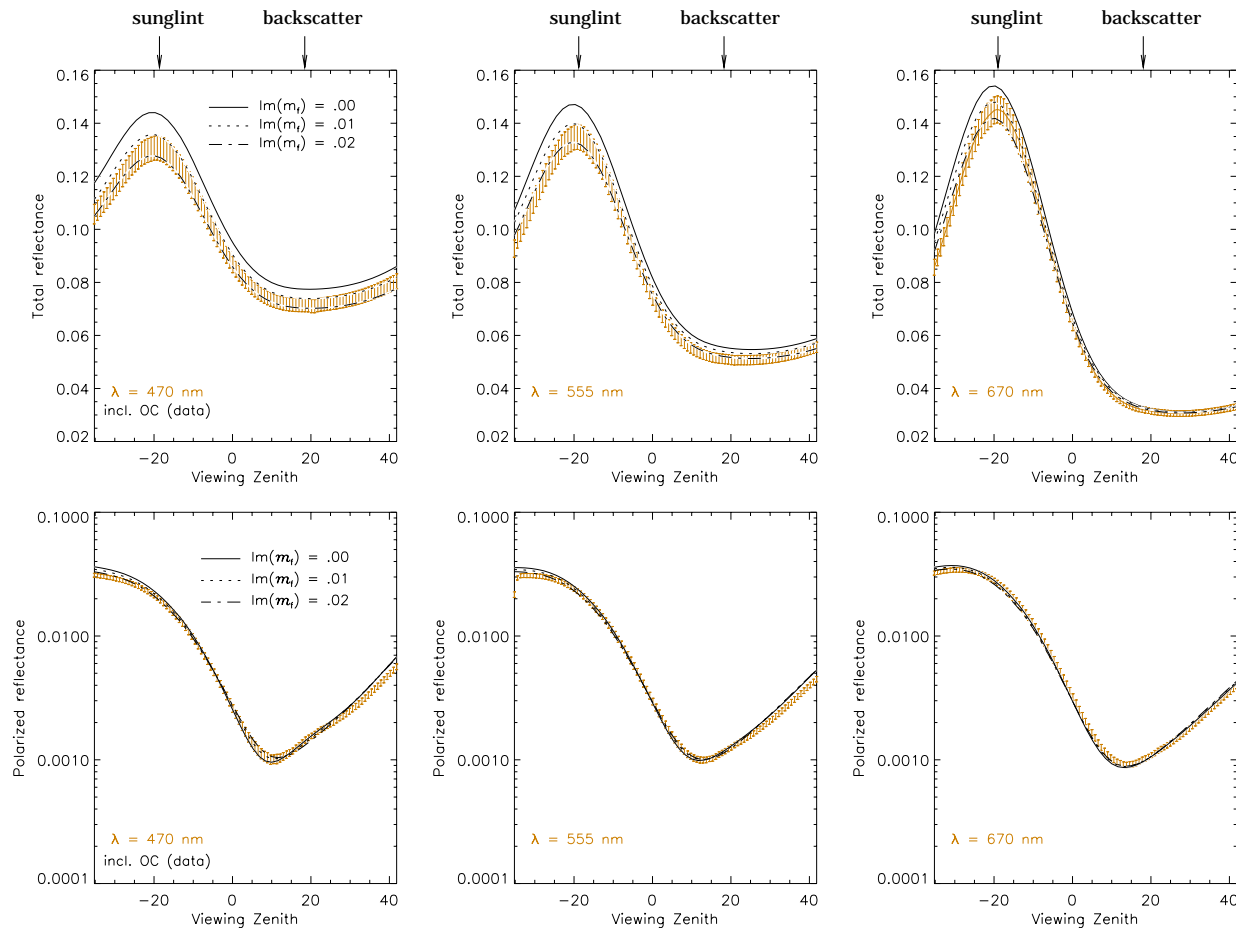


Fig. 4. Analyses of the sensitivity of RSP data to variations in the absorption properties of aerosols. The error bars denote the same combined standard deviations as in Fig. 3. The solid, dotted, and dash-dotted curves are the numerical results for the ocean color derived from underwater light measurements and for the aerosol model specified in Table 1 for $\text{Im}[m_f] = 0.00, 0.01, \text{ and } 0.02$, respectively.

RSP reflectances for all wavelengths. Perturbations in the particle size distribution and/or real refractive index lead, on the other hand, to significant changes in these reflectances which allows for the retrieval of these aerosol properties regardless of the ocean color (step 2 in Sec. 3). Finally, the underwater light contribution computed for $\lambda = 555$ and 470 nm leads to total reflectances that are much larger than the corresponding RSP reflectances. It is possible to reconcile these reflectances by modifying our values for r_e , v_e , and/or τ_f ; however, one can then not obtain satisfying fits for the other RSP reflectances if $\text{Im}[m_f]$ remains fixed at 0.00. We need therefore to consider other values of $\text{Im}[m_f]$ for this aerosol (steps 4–5 in Sec. 3).

The panels in Fig. 4 show the same RSP and numerical reflectances as in Fig. 3 except for varying $\text{Im}[m_f]$ in our computations and adjusting the corresponding estimates for τ_f (step 6 in Sec. 3). The solid, dotted and dash-dotted lines are the results computed for $\text{Im}[m_f] = 0.00, 0.01, \text{ and } 0.02$, respectively. Note for these results that r_e , v_e and $\text{Re}[m_f]$ are kept fixed at their perspective values retrieved for $\text{Im}[m_f] = 0.00$ (Table 1) and that we include contributions from underwater light scattering. The corresponding results for a black ocean are omitted for simplicity. We observe first that the differences in polarized reflectances computed for various $\text{Im}[m_f]$ are smaller than the measurement uncertainty in the corresponding RSP reflectances. That is, we do not need to reevaluate the values retrieved for r_e , v_e and $\text{Re}[m_f]$ if $\text{Im}[m_f]$ is much larger than zero for this aerosol model (step 7 in Sec. 3). Secondly, the total reflectances computed for $\lambda = 555$ and 470 nm are significantly reduced for our non-zero values of $\text{Im}[m_f]$. The change is particularly noticeable for the sunglint reflectances, which is also consistent with the method proposed by Kaufman *et al.*²⁵ to estimate aerosol single scattering albedos from such reflectances. Comparison with the RSP reflectances show

that a reasonable fit can be obtained (step 8 in Sec. 3) if $0.01 \leq \text{Im}[m_f] \leq 0.02$. The corresponding values for $\overline{\omega}_f$ are listed in Table 1, from which we conclude that $\overline{\omega}_f \approx 0.91 \pm 0.03$ in the VIS.

5.2 Validation

We examine first the retrieval of particle size distributions. Using the *in-situ* measurements obtained by a Passive Cavity Aerosol Spectrometer Probe (PCASP) located on the wing of the Convair-580 aircraft, *Magi et al.*²⁶ derive a geometrical mean diameter of $0.19 (\pm 0.02) \mu\text{m}$ for the fine-mode particles on July 17 of the CLAMS campaign. The corresponding value from the RSP retrieval is $0.23 \mu\text{m}$. Note that the PCASP retrievals are for dry particles only, and one would therefore expect the PCASP values to be equal to or smaller than the RSP ones depending on the state of hydration of the ambient particles. Hence, we obtain reasonable agreement for the fine-mode particle size distribution. Similar conclusions can be reached by comparing the fine-mode particle phase function derived from AERONET data with the one computed from the aerosol model retrieved from RSP data (Fig. 5a). Note how these scattering functions agree quite well especially for scattering angles less than 100° , i.e., for scattering angles that are not only typically captured by AERONET observations but that include also observations of the diffraction peak which is particularly sensitive the particle size distribution (cf. Fig. 1a,c).

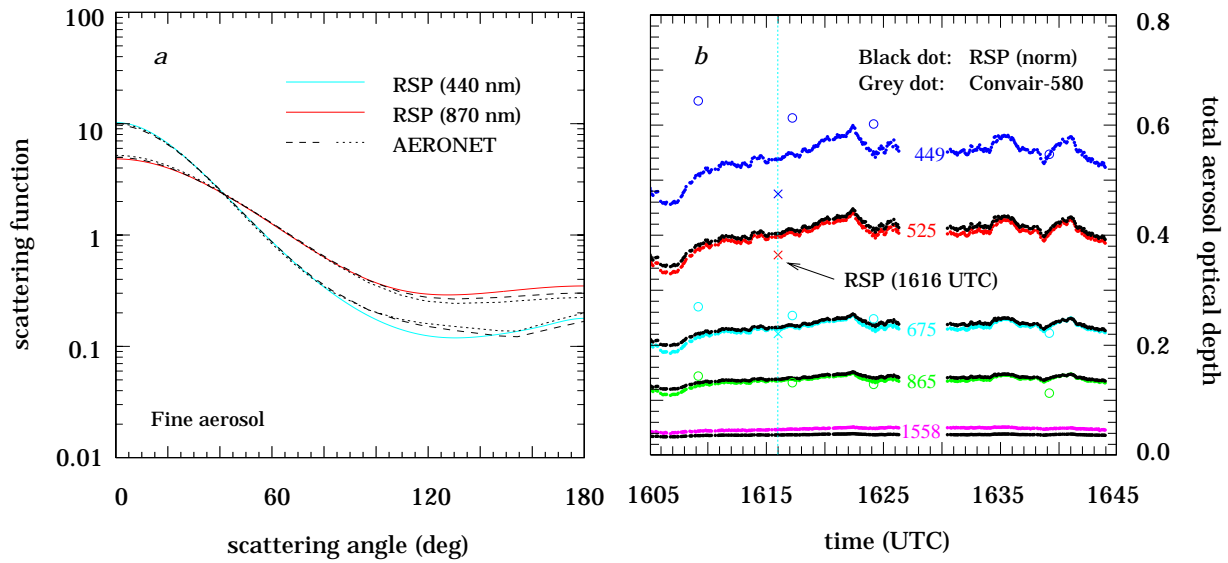


Fig. 5. *a*. Scattering functions for the fine-mode particles derived from RSP data (solid curves), and from AERONET data in the morning (dotted) and afternoon (dashed). The real refractive index $\text{Re}[m_f]$ and imaginary refractive index $\text{Im}[m_f]$ for the RSP retrievals is 1.44 and 0.01, respectively. The RSP results do not change significantly if $\Delta\text{Im}[m_f] = \pm 0.01$ or if $\Delta\text{Re}[m_f] = \pm 0.02$. *b*. The spectral and spatial variations of aerosol optical depth. The colored (grey) dots are the Convair-580 results for $\lambda = 449, 525, 675, 865,$ and 1559 nm . The open circles are the AERONET results for $\lambda = 440, 670 \text{ nm}$ and 870 nm . The crosses are the RSP results for $\text{Im}[m_f] = 0.02$ observed at 1616 UTC and applied to $\lambda = 449, 525,$ and 675 nm . The black dots are the RSP results for $\text{Im}[m_f] = 0.02$ normalized to the convair-580 results at $\lambda = 449$ and applied to $\lambda = 525, 675, 865,$ and 1559 nm .

To evaluate our retrievals for the aerosol optical depth τ_f , we compare in Fig. 5b our results with those retrieved from the AERONET and Convair-580 aircraft sunphotometer data. The crosses in this figure are the RSP retrievals for $\text{Im}[m_f] = 0.02$ (the corresponding results for $\text{Im}[m_f] = 0.01$ are slightly smaller; see Table 1). The circles and colored (grey) curves are the AERONET and Convair-580 retrievals, respectively. We observe that the RSP retrievals are lower than the Convair-580 retrievals while the AERONET retrievals are higher. However, the differences are comparable to the temporal and spatial variations encountered by the Convair-580 aircraft. Indeed, if we use the RSP aerosol model and normalize its optical thickness to the one retrieved from the Convair-580 data at $\lambda = 449 \text{ nm}$, we are able to obtain good fits to the other Convair-580 retrievals up to $\lambda = 865 \text{ nm}$ (see black curves). The discrepancies seen at the largest wavelength can simply be attributed to the presence of coarse-mode particles, which are ignored in the inversion of RSP data for this case study. Hence, our τ_f retrievals agree well with results from sunphotometer analyses.

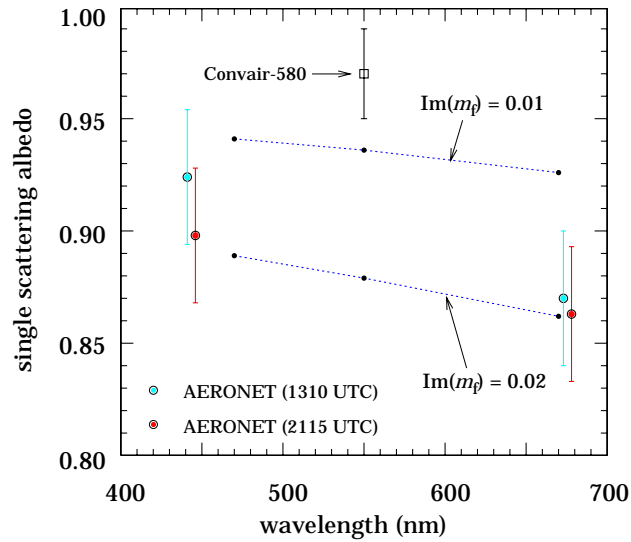


Fig. 6. Single scattering albedo retrievals. The upper and lower lines are the RSP retrievals at 1616 UTC for $\text{Im}[m_f] = 0.01$ and 0.02, respectively. The circles are the AERONET retrievals at 1310 and 2115 UTC. The box is the Convair-580 average for the day. Note that the spectrum of the AERONET retrievals at 2115 UTC has been artificially shifted by 5 nm.

Figure 6 finally compares our retrieval of ω_f with those from the skylight measurements of AERONET and the *in-situ* measurements onboard the Convair-580 aircraft. The upper and lower dotted lines are the RSP-derived spectral variations of ω_f for $\text{Im}[m_f] = 0.01$ and 0.02, respectively. The circles and square are the corresponding results for the AERONET sunphotometer and the Convair-580 nephelometer analyses, respectively. Good agreement can be observed for the RSP and AERONET retrievals; however, the Convair-580 retrieval (0.97 ± 0.02 at $\lambda = 550$ nm) is significantly higher. *Magi et al.*²⁶ mention as possible causes for this discrepancy the loss of particles in the sampling system for the *in-situ* measurements, the considerable horizontal variability in the aerosol burden, and uncertainties in the retrieval of ω_f from AERONET data. Another cause may be that the Convair-580 nephelometer measures the scattering and absorption coefficients of *dried* particles. The scattering coefficients are corrected afterwards for hygroscopic growth effects before retrieving ω_f , but the absorption coefficients are assumed to be independent of relative humidity. Model computations performed by *Redemann et al.*²⁷ suggest that this assumption is often not true and that it may lead to overestimating ω_f by one-to-several hundredths. The distribution of soot within aerosol particles may also be different for hydrated and dried particles, which affects ω_f according to model computations by *Fuller et al.*²⁸. It is therefore conceivable that the uncertainty in the Convair-580 estimate of ω_f is actually larger than reported by *Magi et al.*²⁵, thereby bringing this estimate within consistency of the RSP estimate.

6. CONCLUSIONS

Analyses of polarized reflectances observed in the VIS from altitudes of 3.6 km during RSP flight 027 of the CLAMS campaign show that, on July 17, the fine-mode aerosol consisted particles with an effective radius r_e of $0.15 (\pm 0.025)$ μm , an effective variance v_e of $0.2 (\pm 0.025)$, and a real refractive index $\text{Re}[m_f]$ of $1.44 (\pm 0.02)$ for $470 \leq \lambda \leq 670$ nm. The corresponding total reflectances can be matched if for these particles we use an effective imaginary refractive index $\text{Im}[m_f]$ between 0.01 and 0.02. The corresponding aerosol single scattering albedo varies between 0.94 and 0.88. Comparison with AERONET data show excellent agreement for the single scattering albedo corresponding to $\text{Im}[m_f] = 0.02$. In situ data collected onboard the Convair-580 aircraft favor, on the other hand the RSP retrieval of $\text{Im}[m_f] = 0.01$. Both data sets confirm the RSP retrievals of fine-mode particle size distribution and are consistent with the RSP spectral variation of optical thickness.

The results presented in this paper demonstrate that it is possible to use polarized reflectances to separate aerosol absorption from ocean color variations in the VIS from aircraft observations over the ocean. In an extended

analyses of these results, we discuss further the sensitivity of RSP reflectances to the vertical distribution of fine-mode particles and assess our ability to accurately compute the contribution of waterleaving radiances to such reflectances²⁹. Our analyses illustrate altogether the capability of future polarimeters such as the Aerosol Polarimetry Sensors planned for flight on NPOESS and the NASA Glory mission to robustly and accurately determine aerosol single scattering albedos over the oceans whenever there is a significant fine aerosol burden ($\tau_f > 0.25$ at $\lambda = 555$ nm).

7. ACKNOWLEDGEMENTS

We gratefully acknowledge support from the NASA Radiation Sciences Program managed by Dr. D. Anderson and from NASA's EOS project. Glenn Cota and his team from the Old Dominion University Center for Coastal Physical Oceanography provided further invaluable assistance acquiring and analyzing the ocean optics data. Their efforts were supported by the Japan Aerospace Exploration Agency and NASA's SeaWiFS and SIMBIOS projects. Finally, the CLAMS field experiment was made possible by the efforts of Drs. Bill Smith Jr. and Tom Charlock of the NASA Langley Research Center to whom we are most grateful for the opportunity to participate.

8. REFERENCES

- 1 Hansen, J., and Coauthors, 1995: Low-cost long-term monitoring of global climate forcings and feedbacks. *Climatic Change*, **31**, 247–271.
- 2 Gordon, H. R., 1997: Atmospheric correction of ocean color imaginary in the Earth Observing System era, *J. Geophys. Res.*, **102**, 17,081-17,106.
- 3 Chowdhary, J., B. Cairns, and L. D. Travis, 2002: Case studies of aerosol retrievals over the ocean from multiangle, multispectral photopolarimetric remote sensing data, *J. Atmos. Sci.*, **59**, 383-397.
- 4 Cairns, B., L. D. Travis, and E. E. Russel, 1999: The Research Scanning Polarimeter: calibration and ground-based measurements, *Polarization: Measurements, Analysis, and Remote Sensing*, D. H. Goldstein and D. B. Chenault, Eds., *Proc. SPIE*, **3745**, 186-196.
- 5 Travis, L. D., 1993: Earth Observing Scanning Polarimeter. *Long-Term Monitoring of Global Climate Forcing and Feedbacks*, J. Hansen et al., Eds., *NASA Conf. Publ.* **3234**, 40-46.
- 6 Morel, A., and Maritorena, S., 2001: Bio-optical equations for oceanic waters: A reappraisal, *J. Geophys. Res.*, **106**, 7163-7180.
- 7 Loisel, H., and A. Morel, 2001: Non-isotropy of the upward radiance field in typical coastal (Case 2) waters. *Int. J. Remote Sens.*, **22**, 275–295.
- 8 Redemann, J., and Coauthors, 2004: Suborbital measurements of spectral aerosol optical depth and its variability at sub-satellite grid scales in support of CLAMS. *Submitted to J. Atm. Sci.*.
- 9 Jin, Z., and Coauthors, 2004: radiation measurement and model simulation for the CLAMS experiment. *Submitted to J. Atm. Sci.*
- 10 Holben, B. N., and Coauthors, 1998: AERONET — A federated instrument network and data archive for aerosol characterization. *Remote Sens. Environ.*, **66**, 1–16.
- 11 Hansen, J. E., and Travis, L. D., 1974: light scattering in planetary atmospheres, *Space Sci. Rev.*, **16**, 527-610.
- 12 Chowdhary, J., B. Cairns, and L. D. Travis, 2004: The contribution of waterleaving radiances to polarimetric remote sensing observations over oceans: Model results for case I waters, *submitted to Appl. Opt.*
- 13 Cox, C. and W. Munk, 1954: Statistics of the sea-surface derived from sun-glitter. *J. Mar. Res.*, **13**, 198–227.
- 14 Sancer, M. I., 1969: Shadow-corrected electromagnetic scattering from a randomly-rough ocean surface, *IEEE Trans. Antennas and Propagation*, **17**, 557-585.
- 15 Koepke, P., 1984: Effective reflectance of oceanic whitecaps, *Appl. Opt.*, **23**, 1816-1842.
- 16 Frouin, R., M. Schindling, and P.-Y. Deschamps, 1996: Spectral reflectance of sea-foam in the visible and near-infrared: In-situ measurements and remote sensing applications. *J. Geophys. Res.*, **101**, 14,361–14,371.
- 17 Preisendorfer, R. W., and Mobley C. D., 1986: Albedos and glitter patterns of a wind-roughened sea surface, *J. Phys. Oceanog.*, **16**, 1293-1316.
- 18 Hansen, J. E., 1971: Multiple scattering of polarized light in planetary atmospheres. Part II. Sunlight reflected by terrestrial clouds, *J. Atm. Sci.*, **28**, 1400-1426.
- 19 Morel, A., D Antoine, and B. Gentilli, 2002: Bidirectional reflectance of oceanic waters: accounting for Raman emission and varying particle scattering function. *Appl. Opt.*, **41**, 6289–6306.

- 19 Spinrad, R. W., and J. F. brown, 1986: Relative real refractive index of marine microorganisms: a technique for flow cytometric estimation, *Appl. Opt.*, **25**, 1930-1934.
- 20 Voss, K. J., and E. S. Fry, 1984: Measurements of the Mueller matrix for ocean water, *Appl. Opt.*, **23**, 4427-4439.
- 21 Morel, A., 1974: Optical properties of pure water and pure sea water. *Optical aspects of Oceanography*, N. G. Jerlov and E. Steeman Nielsen, Eds, Academic Press, 1-24.
- 22 Ulloa, O., S. Sathyendranath, and T. Platt, 1994: effect of the particle-size distribution on the backscattering ratio in seawater. *Appl. Opt.*, **33**, 7070–7077.
- 23 Morel, A., and I. Prieur, 1977: Analyses of variations in ocean color. *Limnol. Oceanogr.*, **22**, 709–722.
- 24 Lean, J., 2002: Evolution of the sun’s spectral irradiance since the Maunder Minimum, *Geophys. Res. Lett.*, **27**, 2425–2428.
- 25 Kaufman, Y. J., J. V. Martins, L. A. Remer, M. R. Schoeberl, and M. A. Yamasoe, 2002: Satellite retrievals of aerosol absorption over the oceans using sunglint. *Geophys. Res. Lett.*, **29**, 1928, doi:10.1029/2002GL015403.
- 26 Magi, B. I., P. V. Hobbs, T. W. Kirchsetter, T. Novakov, D. E. Hegg, S. Gao, J. Redemann, and B. Schmid, 2004: Aerosol and chemical apportionment of aerosol optical depth at locations off the United States East coast in July and August 2001. *Submitted to J. Atm. Sci.*
- 27 Redemann, J., P. B. Russell, and P. Hamill, 2001: Dependence of aerosol light absorption and single scattering albedo on ambient relative humidity for sulfate aerosols with black carbon cores. *J. Geophys. Res.*, **106**, 27 485–27 495.
- 28 Fuller, K. A., W. C. Malm, and S. M. Kreidenweis, 1999: Effects of mixing on extinction by carbonaceous particles, *J. Geophys. Res.*, **104**, 15,941-15,954.
- 29 Chowdhary, J., and Co-authors, 2004: Retrieval of aerosol scattering and absorption properties from photo-polarimetric observations over the ocean during the CLAMS campaign, *submitted to J. Am Sci.*